A 2D model for coupled heat, air, and moisture transfer through porous media in contact with air channels

Clément Belleudy, Monika Woloszyn, Marx Chhay, Matthieu Cosnier

A 2D model for coupled heat, air, and moisture transfer through porous media in contact with air channels

Clément Belleudy[a,b,*], Monika Woloszyn[a], Marx Chhay[a], Matthieu Cosnier[b]

[a] *LOCIE, CNRS UMR 5271, Université Savoie Mont Blanc, Campus scientifique Savoie Technolac, Bâtiment Helios, Avenue du Lac Léman, 73376 Le Bourget du Lac, France*

[b] *Centre Scientifique et Technique du Bâtiment (CSTB), 24 rue Joseph Fourier, 38400 Saint Martin d'Hères, France*

Abstract

Detailed modelling of air leakage paths through complex building wall assemblies is a challenging task. It requires transient modelling of diffusion and advection phenomena through fluid and solid domains, including porous materials and air channels. In this article, the development of a numerical model coupling heat air and moisture transfers (commonly called HAM transfers) is presented. The model is able to deal with non-isothermal air flow through complex 2D (two-dimensional) geometries, combining air channels and porous media, air permeable or not. A stepwise 1D validation of the model is achieved with numerical benchmarks. The model is then tested on a 2D air leakage configuration subjected to infiltration and exfiltration scenarii.

Keywords: HAM model, moisture, transient, porous media, air leakage, air channels

1. Introduction

Coupled heat and mass transfers in building components have been an active research topic since the late fifties. After the oil crisis in 1974, successive building codes have been strengthening insulation and airtightness standards. Although these measures have helped to reduce the heat loss, it also made building envelopes more sensitive to moisture related problems.

To address these issues, a large amount of numerical tools were released, providing more accuracy than the well-known Glaser method [1], which has been used since the fifties. Among other references from literature, WUFI [2] and DELPHIN [3] software can be cited, as they are particularly easy to handle for non-expert users. A great amount of experimental data is also available for validating hygrothermal models [4].

Over the past twenty years, experimental work and on site observations brought to light the major influence of air flow on the hygrothermal field [5, 6]. Modelling research work firstly focused on coupling heat and air transfers in building components. It was shown that the infiltration and exfiltration heat loss had an influence on the conduction heat loss because air exchanges heat with the wall components. For infiltrating flows typically measured in residential buildings, not accounting for this heat recovery could lead to overestimate the total heat load between 3% and 13% [7]. Other works showed that forced and natural air convection could significantly change the apparent thermal resistance of loose-fill attic insulation [8, 9]. 3D (three-dimensional) configurations were investigated with air entering the assembly through cracks in the sheathings, forming air paths through the wall assembly [10].

While coupling air with hygrothermal transfers, numerical difficulties may arise because of non linearities and large time constant differences between transfer processes. Successful 1D attempts to couple heat air and mass (HAM) transfers in porous material were achieved by [11] and [12], using relative humidity and suction

*Corresponding author

Email addresses: clement.belleudy@univ-savoie.fr (Clément Belleudy), monika.woloszyn@univ-savoie.fr (Monika Woloszyn), marx.chhay@univ-savoie.fr (Marx Chhay), matthieu.cosnier@cstb.fr (Matthieu Cosnier)

pressure as moisture potential, respectively. Further work was done on realistic 2D and 3D geometries [13, 14], with air entering uniformly through one side of the building assembly.

To deal with coupled HAM transfers in both porous media and air channels, different modelling strategies are reported in the literature: (fig. 1) summarizes the different approaches. There are two major types of modelling approaches: the one-domain approach or the two-domain approach. In the first one, a single set system of transport equations is used in the whole domain including both porous media and air channels, with position dependent coefficients. In the latter, different transport equations are used in each domain (e.g. Darcy law in porous media and Navier stokes equation in air channel), so that an interface condition must be written to connect both computational domains. In this regard, the one-domain approach enable easier numerical implementation, as it only requires one solver to solve the equation over both domains (there is no interface coupling). More detail about these two approaches can be found in [15].

Air transfer computational domains are presented in the first row and those of heat and moisture transfers in the second row. In each domain, indicated by a thick line, transfer processes are ruled by the same partial derivative equations (PDE). Inside certain domains, dotted lines separate areas of different properties.

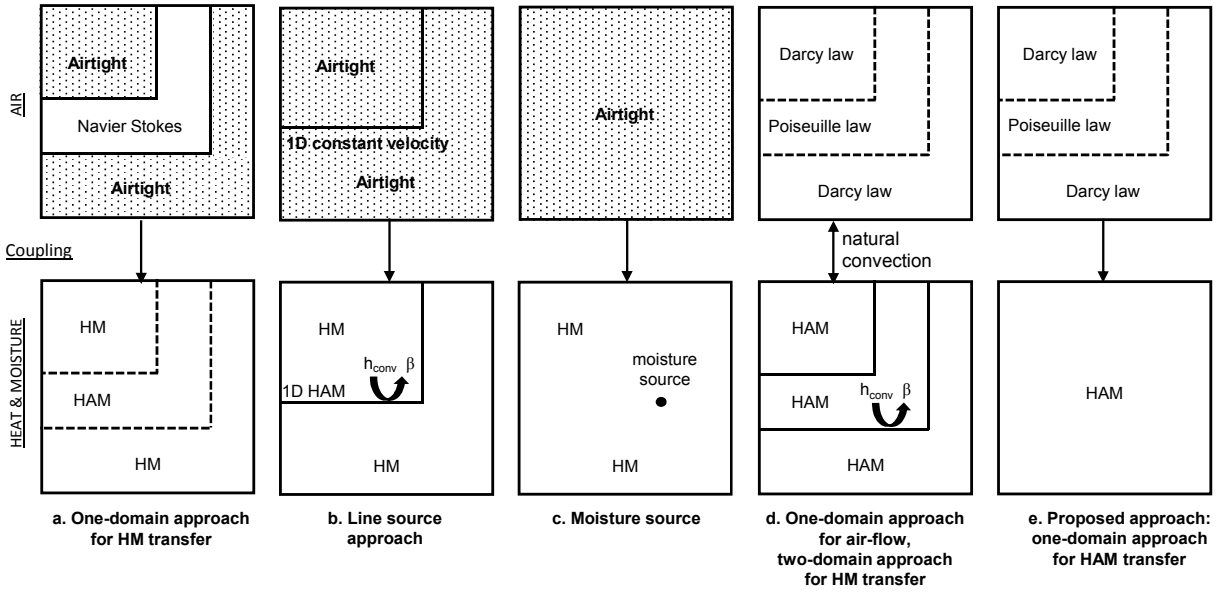

Figure 1: Modelling strategies

In case of air channels in contact with airtight porous materials, [16] compares a one-domain approach (fig. 1a.) and a line source approach (fig. 1b.). The first one consists in solving the velocity field in the air channel alone with CFD codes, and then solving simultaneously hygrothermal transfers in both air gap and porous domains. No surface film coefficient is thus required to couple fluid and airtight porous material. The line source approach (which belongs to two-domain approaches) reduces the computational effort, which is profitable for long-term simulations. The basic principle is to describe the air gap in 1D and calculate a velocity with a macroscopic law such as the power law. Then the convective transfer of moisture and energy can be modelled along the air channel axis with 1D balance equations and surface film coefficients. An overall good agreement is obtained compared to the comprehensive one-domain approach except near bends where vortex effects cannot be captured. The line source approach has been recently used to assess the effect of streaming air between timber beam and masonry [17].

An alternative way to capture the effect of air flow on the hygrothermal field is to add a transient moisture source in the assembly [18]. Air is therefore not modelled as an active component in the assembly. The position of the moisture source must be determined according to practical experience (fig. 1c.).

On site investigations in France [19] proved that leaking air mostly flows through porous materials and thin air channels due to material imperfections and construction tolerances. In addition, air inlet and

outlet are not necessarily close to each other, which makes air leakage paths through the building envelope multidimensional and difficult to map. Very few existing HAM models enable such complex air leakage geometries to be dealt with.

Regarding air gaps in contact with air permeable porous material, one of the most detailed modelling approaches is proposed by [20] and has been recently implemented in DELPHIN by [21]. A one-domain approach is used to compute air velocity field in both air permeable porous material and air channels, with Darcy law and the averaged Poiseuille law, respectively. Natural convection is captured using Boussinesq approximation. Heat and moisture transfers in porous material and air channels are coupled together using constant heat and vapour surface film coefficients along interfaces (fig. 1d.).

For 2D tortuous air gaps, the assumption of simplified boundary conditions at air gaps interfaces implied by a two-domain approach might be questioned as effective values of surface film coefficients vary significantly between rectilinear and bend sections. It is possible to dispense with these boundary conditions by describing HAM transfers continuously in air gaps and porous media with one single system of equations. Such a one-domain approach (fig. 1e.) is proposed in the present paper. This newly-developed HAM model is designated as HAM-Lea ("Lea" standing for "Leakage").

In a first part of the paper, the general governing equations for coupled HAM transfers in both multilayered porous media and air channels are presented, and suitable assumptions are made, leading to the HAM-Lea system of equations. Secondly, a numerical validation of this system is presented, based on published numerical benchmarks. Finally, HAM-Lea is applied to a complex 2D geometry including air channels and porous media, subjected to transient boundary conditions. This last section illustrates the applicability of HAM-Lea to real problems from building physics.

2. Governing equations

HAM transfers are ruled by conservation laws written as PDE. For this purpose, the continuum medium approximation is used: all properties are averaged on representative elementary volumes (REV).

The general form of a conservation law states that the rate of increase of a quantity A in an REV equals the net inflow of this quantity $-\nabla \cdot q_A$ into this REV, plus a source term s:

$$\frac{\partial A}{\partial t} = -\nabla \cdot q_A + s \tag{1}$$

Where q_A is the flux density of the A quantity. Depending on the balance equation, quantity A represents dry air mass, water mass, or energy, respectively. In the following sections, equations for each quantity will be detailed differentiating transport in porous media and in air channels.

2.1. Air

2.1.1. Air flow in porous media

In the porous medium, the general equation for dry air mass conservation, also called continuity equation, reads:

$$\varepsilon \frac{\partial \rho_{air}}{\partial t} = -\nabla \cdot (\rho_{air} u) \tag{2}$$

where ε [$-$] is the open porosity of the porous medium, ρ_{air} [kg/m^3] the dry air density and u [m/s] the Darcy velocity, which is an averaged velocity over a REV. One neglects "source term". The Dupuis-Forchheimer relationship provides the link between the Darcy velocity u and the intrinsic velocity v:

$$u = \varepsilon \times v \tag{3}$$

In building physics, air velocities remain sufficiently low, consequently the assumption of incompressible flow is widely accepted. The continuity equation simplifies to:

$$\nabla \cdot u = 0 \tag{4}$$

The general form of momentum conservation for laminar air flow in porous media is obtained by analogy with the Navier Stokes equation applied to an air volume, with additional drag terms due to the resistance of the rigid porous matrix against the flow. Interested readers may refer to handbooks about heat and mass transfer in fluids and porous media [22, 23] for further details.

$$\underbrace{\frac{\rho_{air}}{\varepsilon}\frac{\partial u}{\partial t}}_{\text{local acceleration}} + \underbrace{\frac{\rho_{air}}{\varepsilon^2}(u\cdot\nabla)(u)}_{\text{advective acceleration}} = \underbrace{-\nabla P}_{\text{pressure force}} \underbrace{+\rho_{air} g}_{\text{body force}} \underbrace{-\mu_{air} k_{mat}^{-1} u}_{\text{Darcy drag term}} \underbrace{-c_F k_{mat}^{-1/2} \rho_{air}|u|u}_{\text{Forchheimer drag term}} \underbrace{+\frac{1}{\varepsilon}\tilde{\mu}\Delta u}_{\text{Brinkman term}} \tag{5}$$

where P [Pa] is the total air pressure, μ_{air} [Pa.s] air dynamic viscosity, $\tilde{\mu}$ [Pa.s] an effective viscosity, k_{mat} [m^2] the material intrinsic permeability, and c_F a dimensionless form-drag constant.

This equation can be simplified, depending on air velocities and the level of detail needed for the simulation. The pore Reynolds number gives information on the flow in the porous medium.

$$Re_p = \frac{L_c \rho_{air} u}{\mu_{air}} \tag{6}$$

The characteristic length L_c [m] for the flow is generally approximated by the square root of the permeability:

$$L_c = \sqrt{k_{mat}} \tag{7}$$

For building physics applications, the flow regime in the porous medium remains laminar. However, the drag term differs depending on the range of Re_p. For $Re_p > 10$ the drag term is quadratic with velocity and thus both Darcy and Forchheimer terms must be considered. In contrast, for Re_p of order of unity, the drag is linear and Darcy term is the only one required.

The Brinkman term is a viscous drag, similar to the laplacian term in the Navier Stokes equation. It is required when the non-slip condition near an impermeable wall interface needs to be captured. An effective viscosity $\tilde{\mu}$ [Pa.s] is introduced, which is close to air dynamic viscosity for high porosity materials. As we do not need a fine description of boundary layer at wall interfaces, Brinkman term will not be considered in our model.

Given the low velocities, the inertial term is usually small compared to the drag terms [22]. Moreover, recent research work proved that it is justified to neglect transient effect of air transport, because of much smaller time scale compared to heat and moisture transport [21]. This assumption is retained for the newly-developed model. For steady state flow, the momentum equation reduces to the general form of the phenomenological Darcy law:

$$u = -\frac{k_{mat}}{\mu_{air}}\left(\nabla P - \rho_{air}(T) g\right) \tag{8}$$

Where g [m^2/s] is the gravitational acceleration vector. The vertical axis (y coordinate) is oriented upwards. The body force, even if small for air in comparison of liquid, is included as it might have a significant contribution on the overall air flow. The body force can be considered as constant, or temperature dependent when natural convection needs to be captured. Natural convection is caused by air density gradient driven by temperature differences. Considering a temperature dependent air density in all conservation equations dramatically increases the system complexity. The Boussinesq approximation allows capturing natural convection restraining density variation to a buoyancy force in the momentum equation as shown in (8).

Within this approximation, air density temperature dependence can be linearized using a Taylor serie near an equilibrium temperature T_0, assuming small variation around this value.

$$\rho_{air}(T) = \rho_{air}(1 - \beta(T - T_0)) \tag{9}$$

with β [K^{-1}] the coefficient of thermal expansion of air. An alternative choice is to use the ideal gas law, using the molar mass of air M_{air} [kg/mol], an equilibrium pressure P_0, the universal gas constant R [J/(mol.K)],

and T the absolute temperature [K]:

$$\rho_{air}(T) = \frac{P_0 M_{air}}{R\,T} \tag{10}$$

Resulting pressure differences across the building envelope are the driving force of air transport. They are due to wind, stack effect and mechanical ventilation. Typical values are within [0-10 Pa] according to [7]. For an order of magnitude, a 160 mm thick layer of highly permeable porous material (glass fiber batt, $\rho_{mat} = 16$ kg/m^3, $k_{mat} = 3.85 \times 10^{-9}$ m^2 [24]) subjected to 10 Pa pressure difference, gives an air velocity of 13 mm/s and a pore Reynolds number of 0.055. This proves the validity of Darcy law for common building materials in standard conditions. Furthermore, as the model is not dedicated to severe weather conditions with temperature gradients over 40°C, we can safely neglect natural convection in porous materials [8]. As a result, Darcy law including a constant body force (8) will be used to calculate the velocity field in porous materials. The expression of Darcy law will be condensed introducing the driving pressure $P^* = P - \rho_{air}\ g\ y$:

$$u = -\frac{k_{mat}}{\mu_{air}} \nabla P^* \tag{11}$$

Disregarding natural convection simplifies the problem as air convection is decoupled from hygrothermal field. This enable the velocity field to be solved prior to the hygrothermal field, which enhances simulation performance, while keeping good precision of results.

2.1.2. Air flow in air channels

The continuity equation (4) describes air mass conservation in thin air channels.

The momentum conservation applied to a fluid particle in motion is the Navier Stokes equation. The variation rate of momentum is equal to the volumic forces applied to this particle, which are hydrostatic pressure, a body force, and a viscous drag due to the fluid viscosity:

$$\rho_{air}\left(\frac{\partial u}{\partial t} + (u \cdot \nabla)(u)\right) = -\nabla P + \rho_{air} g + \mu_{air} \Delta u \tag{12}$$

Equations (12) and (5) are very similar. In air channels the porosity is equal to one and drag terms simplify to $\mu_{air}\Delta u$. As previously mentioned, the transient terms can be safely omitted in (12). As previously, we consider a constant body force, and we do not account for natural convection. This leads to Poiseuille law [25], valid for 2D fully-developed laminar flow in cylindrical pipes or between parallel plates. Considering Cartesian coordinates with the x-axis parallel to the flow direction, and the driving pressure P^*, Poiseuille law may be expressed as:

$$\frac{\partial^2 u}{\partial y^2} = \frac{1}{\mu_{air}} \frac{\partial P^*}{\partial x} \tag{13}$$

In case of a flow between infinite parallel plates, (13) can be integrated as:

$$u(y) = \frac{1}{2\mu_{air}} \frac{\partial P^*}{\partial x} (y^2 - ey) \tag{14}$$

The air channel related Reynolds number is written using the channel thickness e [m] as a characteristic length:

$$Re = \frac{e\ \rho_{air} u}{\mu_{air}} < 2000 \tag{15}$$

The fully-developed flow hypothesis is satisfied far enough from air inlet or air channel bends. If this rectilinear distance is noted L, the following rule can be applied [25]:

$$\frac{L}{e} > 0.05\ Re \tag{16}$$

Assuming that the leaking air velocity is below 0.5 m/s [26] in a 2 mm thick air channel, the resulting Reynolds number is $Re = 67$. According to (16), the condition $L/e > 3$ must be fulfilled to assume fully-developed flow in air channel. This condition holds 7 mm from air inlet or bends. This level of accuracy is deemed to be satisfactory regarding the characteristic lengths of leaking building assemblies (see section 4).

While integrating the parabolic velocity profile (14) over the y-direction, the mean velocity profile can be expressed in the air gap and an equivalent permeability of the air channel appears:

$$u = -\frac{k_{eq}}{\mu_{air}} \nabla P^* \qquad \text{with} \qquad k_{eq} = \frac{e^2}{12} \tag{17}$$

However, the use of Poiseuille law might be questioned while modelling air channels that are in contact with permeable porous material, as the no-slip condition is no longer verified at the interface. The expression of a slip flow boundary condition between the fluid and the air permeable porous medium has been introduced by [27]:

$$\frac{du_f}{dy} = \frac{\alpha_{bj}}{\sqrt{k_{mat}}}(u_{surf} - u_{mat}) \tag{18}$$

where α_{bj} is a dimensionless quantity depending on the structure of the permeable porous material, u_f, u_{mat} and u_{surf} the y-velocity components in the fluid, the material and at the interface, respectively. As a consequence, the predicted flow rate in the air gap and hence the equivalent permeability k_{eq} are greater compared to those calculated with Poiseuille law. While resolving (13) with $u = 0$ and (18) as boundary conditions at both sides of the channel, we obtain the following velocity expression:

$$u = -(1+\phi)\frac{k_{eq}}{\mu}\nabla P \qquad \text{with} \qquad \phi = \frac{3(\sigma + 2\alpha_{bj})}{\sigma(1+\alpha_{bj}\sigma)} \quad \text{and} \quad \sigma = \frac{e}{\sqrt{k_{mat}}} \tag{19}$$

If α_{bj} is assumed of order of unity, as suggested by [27], a 2 mm wide air channel in contact with a highly permeable porous material (glass fiber batt, $\rho_{mat} = 16$ kg/m^3, $k_{mat} = 3.85 \times 10^{-9}$ m^2 [24]) gives $\phi \approx 0.1$, which corresponds to an air flow increase in 10 % compared those calculated with (13). This is an extreme case: for less permeable insulation material ($k_{mat} \approx 10^{-10}$ m^2), this flowrate increase stays below 3 %. As we are firstly interested in the magnitude order of this flowrate, Poiseuille law will be used in the model to calculate the equivalent permeability of the air channel.

2.1.3. Boundary conditions

Boundary conditions are straightforward: air pressure or air velocity may be applied on air inlets, and a reference pressure at the air outlet. In most cases, resulting pressure differences between indoor and outdoor can be measured on field. Sometimes, air inlet velocity is easier to access, in particular for experimental setups where air flow is supplied by a sample pump at a controlled rate through an airtightness defect [28]. Whether pressure or velocity is imposed at air inlet, it is of importance to set a reference pressure elsewhere in the domain to ensure that the problem is well-posed. A slip boundary condition is written on airtight boundaries:

$$u \cdot n = 0 \tag{20}$$

where n is the outward-pointing normal vector.

2.2. Moisture

2.2.1. Moisture transport in porous media

The conservation equation for moisture transfer reads:

$$\frac{\partial w(\varphi)}{\partial t} = -\nabla \cdot g_{diff} - \nabla \cdot g_{adv} - \nabla \cdot g_{liq} \tag{21}$$

Where w [kg/m^3] is the material moisture content, φ the air relative humidity, and g_{diff}, g_{adv}, g_{liq} the moisture diffusion, advection and capillary suction flux densities, respectively, expressed in [kg/(s.m^2)]. The storage term $\partial w(\varphi)/\partial t$, can be derived from the sorption curve mentioned below.

Moisture transfer consist of three main phenomena: vapour diffusion, vapour advection by air flow, and capillary suction. The moisture diffusion flux, ruled by Fick law, is pointing in the opposite direction of the vapour pressure gradient:

$$g_{diff} = -\delta_{mat}(\varphi)\nabla p_v(T,\varphi) \tag{22}$$

p_v [Pa] is the partial pressure of water vapour and δ_{mat} [s] the vapour permeability of the material. In order to make this property more meaningful, the ratio between air vapour permeability δ_0 and δ_{mat}, called the vapour resistance factor or $\mu - factor$, is often used:

$$\mu - factor(\varphi) = \frac{\delta_0}{\delta_{mat}(\varphi)} \tag{23}$$

δ_{mat} and $\mu - factor$ depend on relative humidity φ. Air is considered as an ideal gas mixture containing dry air and water vapour. Water vapour carried by air flow is referred as advected moisture flow:

$$g_{adv} = \rho_{vap}(T,\varphi)u \tag{24}$$

ρ_{vap} [kg/m^3] is the water vapour content of air, also called humidity by volume. According to ideal gas law:

$$\rho_{vap}(T,\varphi) = \frac{M_w}{RT}\, p_v(T,\varphi) \tag{25}$$

Liquid water transport occurs firstly in smaller pores subjected to capillary condensation, which generates a suction pressure gradient. This liquid flow, namely capillary suction flow, can be expressed with a Darcy law, as in (11):

$$g_{liq} = -K_l(\varphi)\nabla P_{suc} \tag{26}$$

where K_l [s] is called the liquid water permeability of the material. Suction pressure is the pressure difference between liquid and vapour phases. Kelvin law states the equilibrium between both phases on the pore scale. Similarly to [29], P_{suc} will be considered as a function of relative humidity only. $T_{ref} = 298.15$ K is commonly chosen as reference temperature. The validity of this assumption will be assessed thanks to numerical benchmarks presented in the next section.

$$P_{suc}(\varphi) = \frac{\rho_w R}{M_w} T_{ref}\, \ln \varphi \tag{27}$$

where ρ_w [kg/m^3] is the density of liquid water and M_w [kg/mol] its molar mass. Capillary suction flow can also be expressed with moisture content or relative humidity as potential:

$$g_{liq} = -D_w(\varphi)\nabla w(\varphi) = -D_w(\varphi)\frac{\partial w(\varphi)}{\partial \varphi}\nabla\varphi \tag{28}$$

where $D_w(\varphi)$ [m^2/s] is the moisture diffusivity. It can be experimentally measured and corresponding values for common building materials are available in literature.

To avoid numerical problems, it is of importance to ensure the continuity of the dependent variables across material interfaces, that is the reason why relative humidity is chosen as driven potential for all moisture transfers.

The relative humidity is defined as the ratio of the partial vapour pressure to the saturation vapour pressure P_{sat} [Pa]:

$$p_v(T,\varphi) = \varphi P_{sat}(T) \tag{29}$$

Among the different existing correlations to calculate $P_{sat}(T)$, the following one from [30] has been implemented in HAM-Lea:

$$P_{sat}(T) = \varphi \times \exp\left(23.5771 - \frac{4042.9}{T - 37.58}\right) \tag{30}$$

The sorption curve gives the equilibrium moisture content in a material in contact with surrounding moist air. Within typical temperature range considered in building physics, temperature impact on the sorption curve can generally be omitted. It is thus measured at $T_{ref} = 298.15$ K and called the sorption isotherm. In addition, for the sake of simplification, no hysteresis phenomena will be considered between absorption and desorption.

By replacing flux expressions (22), (24) and (28) in (21) and rewriting the equation with relative humidity as moisture state variable, the moisture conservation equation can be formulated using a general coefficient form PDE:

$$d_a \frac{\partial \varphi}{\partial t} + \nabla \cdot (-c\nabla\varphi - \alpha\varphi + \gamma) + \beta\nabla\varphi + a\varphi = f \tag{31}$$

The different coefficients are given below:

$$\begin{aligned}
d_a &= \frac{\partial w(\varphi)}{\partial \varphi} \\
c &= \delta_{mat}(\varphi) P_{sat}(T) + \frac{K_l(\varphi)\rho_w R T_{ref}}{\varphi M_w} \\
\text{or} \quad c &= \delta_{mat}(\varphi) P_{sat}(T) + D_w(\varphi)\frac{\partial w(\varphi)}{\partial \varphi} \\
\alpha &= \delta_{mat}(\varphi)\frac{\mathrm{d}P_{sat}(T)}{\mathrm{d}T}\nabla T \\
\gamma &= 0 \\
\beta &= \frac{M_w P_{sat}(T)}{RT}\, u \\
a &= \frac{M_w \nabla T \cdot u}{R}\left(\frac{1}{T}\frac{\mathrm{d}P_{sat}(T)}{\mathrm{d}T} - \frac{P_{sat}(T)}{T^2}\right) \\
f &= 0
\end{aligned} \tag{32}$$

2.2.2. Moisture transport in air channels

Moisture transport in air channels is mainly due to advection by air movements and to vapour diffusion in air. Moreover, as water content of air is generally several orders of magnitude lower than water content in materials, we can therefore assume a negligible dependency of water vapour content of air to the temperature, i.e. $\partial \rho_{vap}/\partial T = 0$.

The general coefficient form PDE is identical to (31), and the different coefficients read:

$$\begin{aligned}
d_a &= \frac{M_w}{RT} P_{sat}(T) \\
c &= \delta_0 P_{sat}(T) \\
\alpha &= \delta_0 \frac{\mathrm{d}P_{sat}(T)}{\mathrm{d}T}\nabla T \\
\gamma &= 0 \\
\beta &= \frac{M_w P_{sat}(T)}{RT} u \\
a &= \frac{M_w \nabla T \cdot u}{R}\left(\frac{1}{T}\frac{\mathrm{d}P_{sat}(T)}{\mathrm{d}T} - \frac{P_{sat}(T)}{T^2}\right) \\
f &= 0
\end{aligned} \tag{33}$$

where δ_0 [s] is the vapour permeability of air.

2.2.3. Boundary conditions

At air inlets, the most straightforward condition is to impose relative humidity. We denote u_{inlet} the inlet velocity, φ_{amb} and φ_{surf} the interior ambient and surface relative humidity, respectively:

$$\varphi_{surf} = \varphi_{amb} \tag{34}$$

Alternatively, the inward moisture flux can be imposed. It is useful for instance when a moisture flux due to driving rain must be included. Written with the formalism of (31), with β_{amb} [s/m] as the surface film coefficient for vapour transfer, it reads:

$$\begin{aligned} -n \cdot (-c\nabla\varphi - \alpha\varphi + \gamma) = \\ \beta_{amb} \left[p_v(T_{amb}, \varphi_{amb}) - p_v(T_{surf}, \varphi_{surf}))\right] \\ +u_{inlet} \left[\rho_{vap}(T_{amb}, \varphi_{amb}) - \rho_{vap}(T_{surf}, \varphi_{surf})\right] \end{aligned} \tag{35}$$

where T_{amb} is the ambient temperature, T_{surf} the surface temperature. The velocity related term is often omitted by researchers [12, 13, 21], because it is small compared to the others in case of air tight materials in combination with low pressure differences.

At air outlets, air exits at the boundary relative humidity, which gives the following boundary condition:

$$-n \cdot (-c\nabla\varphi - \alpha\varphi + \gamma) = \beta_{amb} \left[p_v(T_{amb}, \varphi_{amb}) - p_v(T_{surf}, \varphi_{surf}))\right] \tag{36}$$

This boundary condition also holds for air tight moisture permeable interfaces. On vapor tight boundaries, the inward moisture flux is zero:

$$-n \cdot (-c\nabla\varphi - \alpha\varphi + \gamma) = 0 \tag{37}$$

2.3. Heat

In the general case, a two-temperature approach must be adopted when dealing with REV containing both solid and gaz phases. In this case, methods exist to determine the interfacial convective heat transfer coefficient in porous media [31]. In building physics area, given low leakage rates and high porosities of air permeable materials, thermal equilibrium between air and solid material is attained within a small distance compared to the wall dimensions, as demonstrated by [32]. Therefore, it is justified to use a one-temperature approach, and thus only one equation for energy conservation.

2.3.1. Energy conservation in porous media

Total energy is the sum of internal, kinetics and potential energy. In building physics, kinetics and potential energy variation are commonly neglected in calculations. Moreover, given low pressure differences, the following approximation can be made:

$$\mathrm{d}U = \mathrm{d}(H - \frac{P}{\rho_{air}}) \approx \mathrm{d}H \tag{38}$$

Where H is the enthalpy of an REV and U its internal energy. Its expression can be written differently whether the REV contains porous medium (39) or air (40). In the following expressions, c_w [J/(kg.K)] and c_{mat} are the heat capacities of liquid water and dry material, respectively. ρ_{mat} [kg/m^3] is the density of dry material, $c_{p_{air}}$ the heat capacity at constant pressure of dry air.

$$\mathrm{d}H = \left[\rho_{mat}c_{mat} + w(\varphi)c_w\right]\mathrm{d}T \tag{39}$$

$$\mathrm{d}H = \rho_{air}c_{p_{air}}\mathrm{d}T \tag{40}$$

The enthalpy variation rate of a REV is driven by three flux densities, namely heat conduction q_{cond}, heat convection by dry air q_{conv}, latent and sensible heat carried by moisture q_{moist}, expressed in [W/m^2].

$$\frac{\partial H}{\partial t} = -\nabla \cdot q_{cond} - \nabla \cdot q_{conv} - \nabla \cdot q_{moist} \tag{41}$$

According to Fourier law, the conductive flux reads:

$$q_{cond} = -\lambda_{mat}(\varphi)\nabla T \tag{42}$$

where $\lambda_{mat}(\varphi)$ [W/(m.K)] is the thermal conductivity of the medium and depends on moisture. q_{conv} is the heat flux density due to dry air convection.

$$q_{conv} = \rho_{air} c_{p_{air}} T\ u \tag{43}$$

The total moisture flow $g_{moist} = g_{diff} + g_{adv} + g_{liq}$ causes both sensible and latent heat fluxes, which are sometimes included in a source term, as shown in (1). The flux density due to latent and sensible heat carried by moisture reads:

$$q_{moist} = g_{liq}\ c_w\ T + (g_{adv} + g_{diff})(c_{p_{vap}} T + L_v) \tag{44}$$

L_v [J/kg] is the moisture latent heat of sorption approximated by the vapour latent heat of evaporation. $c_{p_{vap}}$ [J/(kg.K)] is the heat capacity at constant pressure of water vapour.

Following literature, HAM-Lea model neglects the sensible part compared to the latent part [33]. In this case the heat flux density due to moisture reduces to:

$$q_{moist} = q_{latent} = L_v(g_{adv} + g_{diff}) \tag{45}$$

Replacing the different fluxes in (41) gives:

$$d'_a \frac{\partial T}{\partial t} + \nabla \cdot (-c'\nabla T - \alpha' T + \gamma') + \beta'\nabla T + a' T = f' \tag{46}$$

$$\begin{aligned}
d'_a &= \rho_{mat}\left(c_{mat} + \frac{w(\varphi)}{\rho_{mat}} c_w\right) \\
c' &= \lambda_{mat}(\varphi) + L_v \delta_{mat}(\varphi)\varphi \frac{\mathrm{d}P_{sat}(T)}{\mathrm{d}T} \\
\alpha' &= 0 \\
\gamma' &= -L_v \delta_{mat}(\varphi) P_{sat}(T) \nabla\varphi \\
\beta' &= \left(\rho_{air} c_{p_{air}} + \frac{L_v M_w \varphi}{RT}\frac{\mathrm{d}P_{sat}(T)}{\mathrm{d}T} - \frac{L_v M_w \varphi P_{sat}(T)}{RT^2}\right) u \\
a' &= 0 \\
f' &= -\frac{L_v M_w P_{sat}(T)}{RT} u \cdot \nabla\varphi
\end{aligned} \tag{47}$$

2.3.2. Energy conservation in air channels

In air channels, energy conservation is obtained directly from (46) considering air as material. Differing coefficients are given below:

$$\begin{aligned}
d'_a &= \rho_{air} c_{p_{air}} \\
c' &= \lambda_0 + L_v\ \delta_0\ \varphi\ \frac{dP_{sat}(T)}{dT} \\
\gamma' &= -L_v \delta_0 P_{sat}(T) \nabla\varphi
\end{aligned} \tag{48}$$

Coefficients α', β', a' and f' are identical to those in (47). The thermal conductivity of dry air is noted λ_0.

2.3.3. Boundary conditions

Similarly to moisture boundary conditions, temperature (49) or inward heat flux (50) can be imposed at air inlets:

$$T_{surf} = T_{amb} \tag{49}$$

or

$$\begin{aligned} -n \cdot (-c'\nabla T - \alpha' T + \gamma') = h_{amb}(T_{amb} - T_{surf}) \\ +L_v \beta_{amb} \left[p_v(T_{amb}, \varphi_{amb}) - p_v(T_{surf}, \varphi_{surf}) \right] \\ +\rho_{air} c_{p_{air}} u_{inlet} (T_{amb} - T_{surf}) \\ +L_v u_{inlet} \left[\rho_{vap}(T_{amb}, \varphi_{amb}) - \rho_{vap}(T_{surf}, \varphi_{surf}) \right] \end{aligned} \tag{50}$$

As for moisture boundary conditions, the velocity related term is often disregarded by researchers. At air outlets, the boundary condition reduces to:

$$\begin{aligned} -n \cdot (-c'\nabla T - \alpha' T + \gamma') = h_{amb}(T_{amb} - T_{surf}) \\ +L_v \beta_{amb} \left[p_v(T_{amb}, \varphi_{amb}) - p_v(T_{surf}, \varphi_{surf}) \right] \end{aligned} \tag{51}$$

This boundary condition also holds for non adiabatic moisture permeable interfaces.

2.4. Numerical tool

The developed numerical model is implemented in the commercial simulation software COMSOL Multiphysics [34] which is manipulated via its user-friendly GUI (Graphic User Interface). The user can either built a geometry directly or import a CAD-file. Constant material properties and values can be entered as parameters, and variable coefficients can be defined either as analytical functions or as a list of discrete values generating interpolated functions. Conservations laws, written as PDEs (eqs. 11,17,31,46), are affected to each domain (various materials, air channels), and the values of the corresponding coefficients are entered. The mesh can be generated directly from the GUI, and it is possible to refine mesh in regions where steep gradients are expected. As indicated previously, disregarding natural convection enables the stationary air flow balance to be solved prior to the transient moisture and energy balance. The resulting velocity field can be used while solving coupled heat and moisture equations. Heat and moisture equation are solved simultaneously with COMSOL's built-in time-dependent solver. It is based on the finite element method and an explicit scheme with variable time stepping. It is possible to define a maximum timestep, coinciding with the one of transient boundary conditions. When convergence issue arise, it can be useful to adjust some of the solver settings such as damping factor, relative tolerance, maximum number of iterations.

3. Benchmarking of the model

In the previous sections, coupled HAM equations implemented in HAM-Lea model were presented. Now, in order to gain confidence in model results, a validation of HAM-Lea using published benchmarks is achieved. They have been developed in the framework of the European HAMSTAD project, which aimed to standardize HAM calculation methods [29]. Three benchmark cases have been chosen, and a step by step methodology was followed for this validation, adding physical processes and coupling terms one after another. A more comprehensive description of used material properties can be found in [29].

3.1. Homogeneous wall

In this benchmark, a monolayer wall is maintained at a constant temperature $T_0 = 20°C$. Thus, moisture and energy equations are no longer coupled, which enables the moisture equation to be solved analytically. The initial relative humidity of the material is $\varphi = 0.95$, corresponding to an initial moisture content of $w = 84.8$ kg/m^3. At $t = 0$, relative humidity falls to $\varphi = 0.45$ on the exterior side and $\varphi = 0.65$ on the interior side, corresponding to a moisture content of 19.5 kg/m^3 and 30.5 kg/m^3 respectively. Heat surface

film coefficient of 25 W/(m^2.K) and moisture surface film coefficient of 1.0×10^{-3} s/m are applied on both exterior and interior sides. Water content profiles in the wall simulated with the model are compared with analytical solutions provided by the benchmark at 100 h, 300 h and 1000 h, as presented in (fig. 2). On this figure, exterior and interior side of the monolithic structure is on the left side and on the right side of the x-axis, respectively. Excellent agreement is found between analytical and simulated profiles.

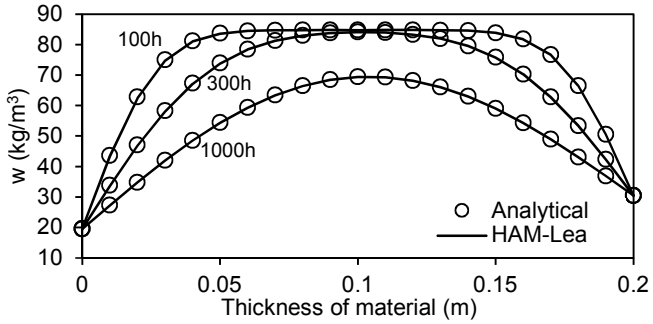

Figure 2: Comparison between analytical solution and HAM-Lea outputs. The interior side is located

3.2. Insulated roof

This benchmark pushes the model validation a step further as a two-layer wall is subjected to transient thermal and moisture conditions. This case originally aims to assess the model ability to predict interstitial condensation between materials. A load bearing wall is insulated on the interior side and a vapor barrier is placed on the exterior side. The whole structure is perfectly airtight. Materials have different moisture properties: the load bearing material is hygroscopic and capillary active whereas the insulation material is less hygroscopic and not capillary active. The simulation is performed over four years. One year transient boundary conditions are repeated every year. The total moisture content in the load bearing material computed by HAM-Lea is plotted in the fifth year, and compared with results obtained by different universities and research institutes, as presented on (fig. 3). The simulated results are contained within the envelope formed by the other plots, which proves good performance of the model.

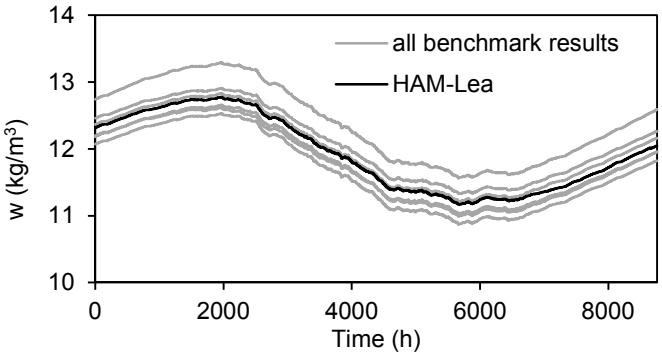

Figure 3: Total moisture content in the load bearing material during the fifth year

3.3. Lightweight wall

In this third and last studied benchmark case, air transfer is finally coupled to hygrothermal transfers. In addition to vapour diffusion and liquid water transport, moisture can be advected by air flow. The internal side of a 200mm thick wall is air and vapour permeable, whereas the external side is air permeable but

vapour tight. During the first 20 days (i.e. 480h) an exfiltration is simulated: air flows from the interior to the exterior side. Afterwards, from the 20th to the 100th day, air direction is reversed to simulate an infiltration. (fig. 4) pictures the moisture content at $x = 0.1$ m against time. It can be seen that the material stores moistures when air exfiltrates because this moisture cannot exit on the exterior side. On the contrary, a drying of the wall occurs in the infiltration phase. An excellent agreement is obtained between the benchmark and the model.

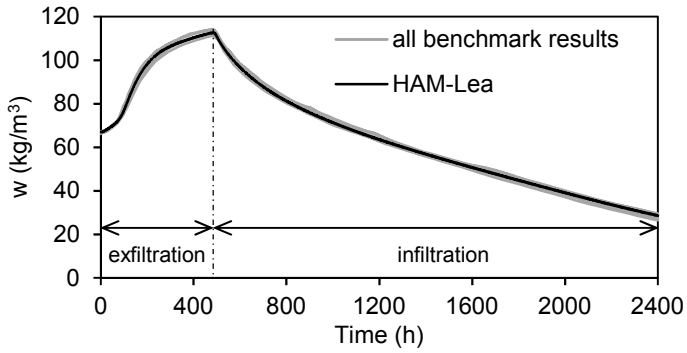

Figure 4: Moisture content at x=0.1 m during 100 days

4. HAM transfers through porous media and air channels: a case study

4.1. Configuration

After validating the model equations, it is proposed to investigate coupled HAM transfers in a complex configuration including porous media – air permeable or not – and thin air channels. In this regard, a typical envelope leakage encountered in wooden-frame buildings is chosen as case study [35]. 2D vertical section gives the composition (fig. 5) and the dimensions of the studied configuration. Thermal insulation is wood fiberboard except near the concrete slab where XPS is used. As a consequence of poor workmanship, flexible sealing may be overlooked and the vapour barrier not sealed properly, which may lead to potential air leakage path between the wood bottom wall plate and the foundation wall. A potential 2 mm air gaps created by tolerances between materials links both the interior and the exterior sides. The vapour barrier has been removed to reproduce the effect of strong discontinuities. Another approximation is done regarding the thermal insulation layer located between vertical studs. As it is not directly subjected to air pressure gradient, it has been considered as airtight to limit the air computation domain. These assumptions allow us to have clearly defined air inlets, oulets, as well as an air computational domain for the simulation (fig. 6). It is assumed that concrete, wood and XPS insulation layers are airtight as well. As natural convection is not taken into account, the velocity can be solved prior to energy and moisture equations. As XPS insulation is neither hygroscopic nor capillary active, its water content was set equal to air water vapour content. Material properties from Fraunhofer-IBP available in WUFI 4 are used ([33] and see appendix). This defect configuration is subjected to transient moisture and thermal boundary conditions. Simulations are performed on long time durations (four years) for infiltration and exfiltration scenarii with different air flow rates.

4.2. Boundary conditions and solver settings

To simulate potentially problematic conditions, a high moisture scenario from WUFI weather database is used. It includes both temperature and relative humidity variations over a year (fig. 7). No external moisture flux due to driving rain is considered. The relative humidity is set at 0.8 as initial value for the whole building assembly. As long term behaviour is of interest here, mean annual variations of temperature and relative humidity are considered. They are described by analytical functions, and presented in (fig. 7

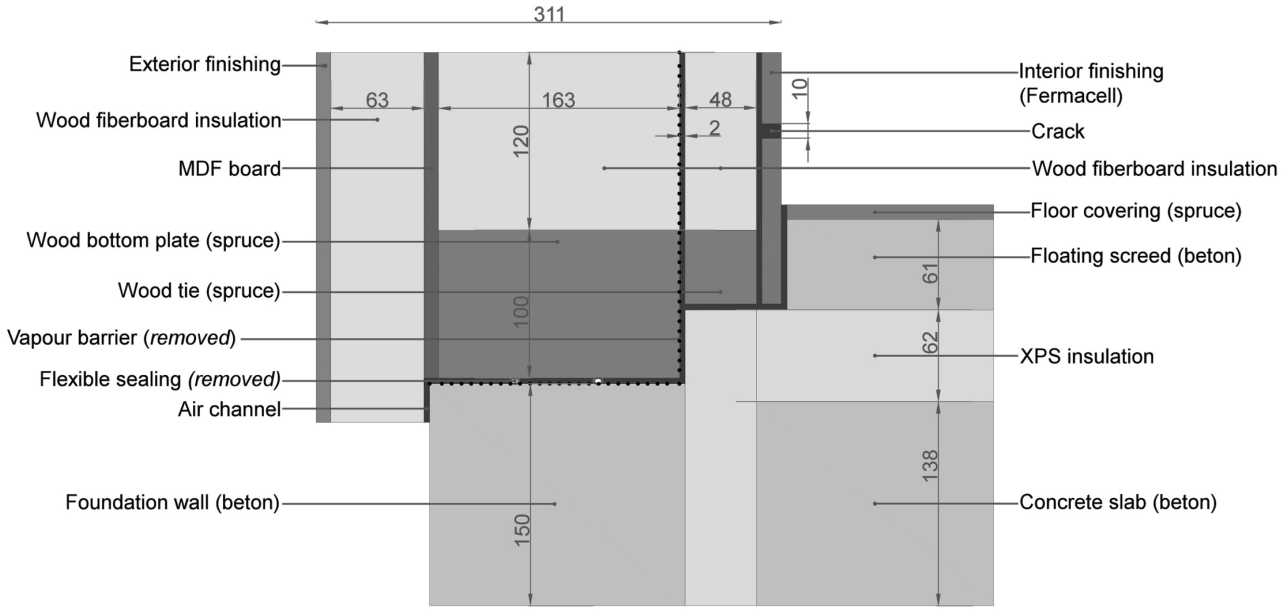

Figure 5: Materials and dimensions in millimetres of the studied section

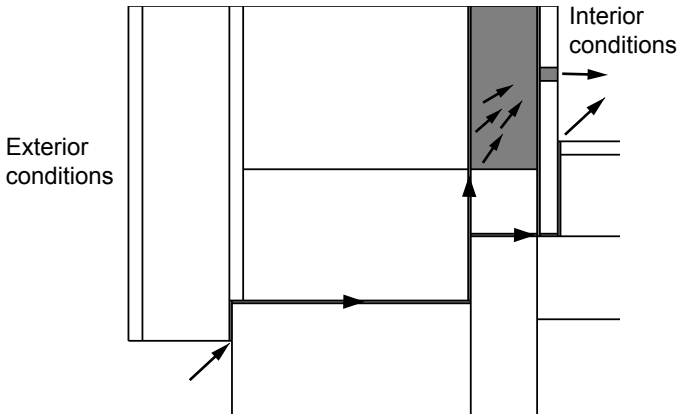

Figure 6: Computed fluid domain and air path for an infiltration scenario

and 8). The initial temperature is set at $[T_{int}(t=0)+T_{ext}(t=0)]/2 = 10°\text{C}$ for the whole building assembly. As described in section 2, prescribed boundary conditions are adopted at air inlets for both moisture and heat equations. Heat and moisture surface film coefficients are applied on interfaces in contact with ambient air. Typical moisture film coefficients suggested by [30] are used:

$$\beta_{int} = 18.5 \cdot 10^{-9} \text{ s/m} \qquad \beta_{ext} = 140 \cdot 10^{-9} \text{ s/m} \tag{52}$$

Heat surface film coefficients are drawn from EN Standards [30]:

$$h_{int} = 7.7 \text{ W/(m}^2\text{.K)} \qquad h_{ext} = 25 \text{ W/(m}^2\text{.K)} \tag{53}$$

Pressure differences is set between air inlets and outlets. Two pressure differences will be tested, resulting in two flow rates. As previously mentioned, pressure differences across the envelope are in general lower

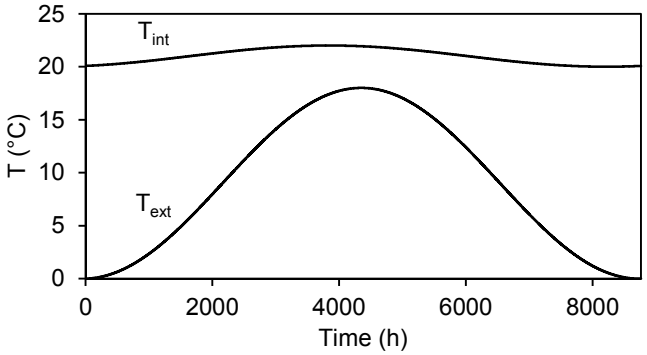

Figure 7: Inside and outside temperatures over a year

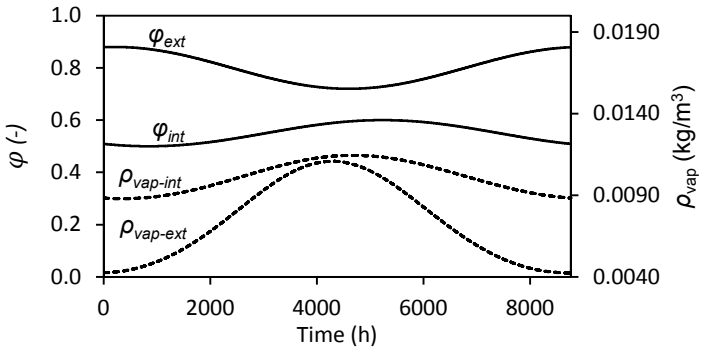

Figure 8: Inside and outside air humidities

than 10 Pa, and smaller values are more likely to be maintained over long periods of time. That is why 0.1 Pa and 1 Pa were chosen as pressure differences for the simulations. If we calculate the velocity field using Darcy's law and Poiseuille's law as described in section (2.1), we do not obtain the same flow rate in infiltration and exfiltration for a given pressure difference $|P_{inside} - P_{outside}|$. This is due to the gravity force, which creates an hydrostatic pressure corresponding to the weight of an air column. As the orifice of the air gap in the exterior side is lower than those in the interior side, the weight of the air column acts from the top down, and generates an air flow from the interior side to the exterior side. This contribution is permanent, even if $|P_{inside} - P_{outside}| = 0$. In order to fairly compare the impact of air flow on HAM transfer in infiltration and exfiltration, it is of importance to have the same flow rate for both cases, for a given pressure difference. This is the reason why, even if the gravity creates a significant contribution in the overall air flow, we will not take it into account it in the following analysis. In exfiltation, when gravity is included, the predicted flow rate is twice as high as the one when gravity is disregarded. Therefore, even if the considered flow rate are biased compared to the real ones, they remain in the same order of magnitude, which maintains the relevancy of this analysis. Omitting gravity finally leads to total flowrates of 0.04 m^3/h and 0.4 m^3/h, for pressure differences of 0.1 Pa and 1 Pa, respectively. For each flow rate, both infiltration and exfiltration scenario are tested. The simulation is performed over 4 years. During the first year, there is no air flow: only heat and moisture diffusion occur. At the end of the first year, pressure differences are applied, generating air flow through the wall assembly.

The hygrothermal field at the end of the first year is used as initial conditions for 3-year exfiltration and infiltration simulations. An overview of the simulation scheme is provided in (fig. 9). Boundary conditions are summarized in (fig. 10).

The geometry has a total of 250,000 meshes built with COMSOL meshing built-in interface. The meshing is refined in narrow regions and in regions where high gradient are expected, for instance in the vicinity of

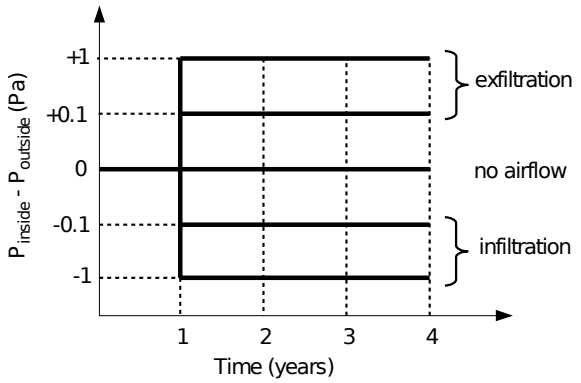

Figure 9: Pressure boundary conditions for all five scenarii

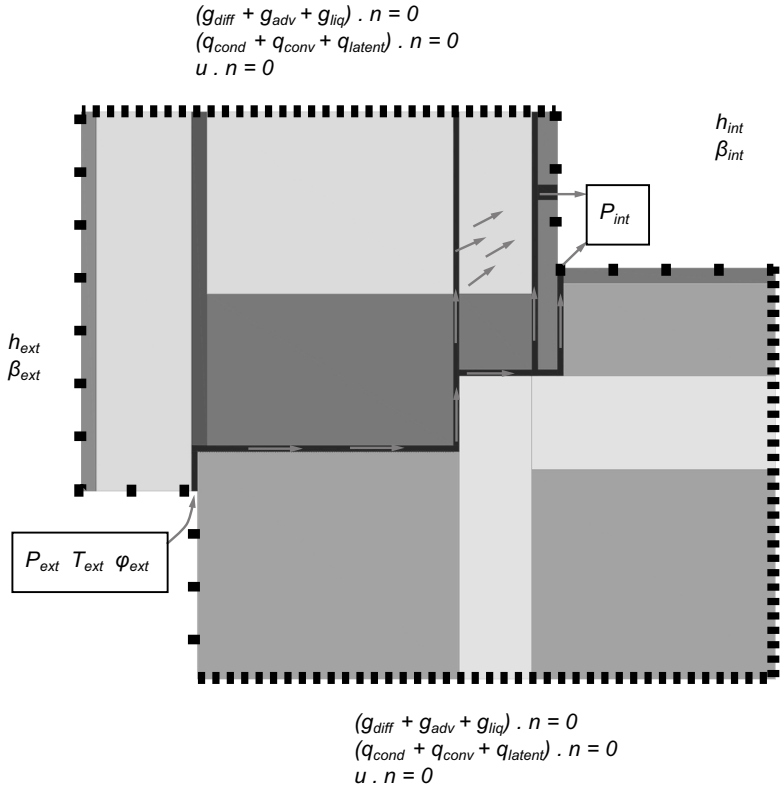

Figure 10: Boundary conditions in case of infiltration

the air channel and on interfaces with ambiant air. The HAM model requires on average 2 hours to run an annual simulation, using an Intel Xeon E5-1650 CPU v2 at 3.5 GHz and 128 GB RAM workstation. Only 5 GB RAM are required to run the simulation.

4.3. Results and discussion

To assess the impact of air flow on the hygrothermal field in the building component, the considered indicator is the averaged moisture content of the wood bottom plate (fig. 5). This rectangular area appeared to be particularly impacted by the air flow, hence the relevancy of this choice. The averaged moisture content

of the wood bottom plate can be calculated as follows:

$$w_{moy}(t) = \frac{\iint_S w(x,y,t)\ \mathrm{d}x\ \mathrm{d}y}{S} \tag{54}$$

where S is the surface of the section.

Plots in (fig. 11) and (fig. 12) show this averaged moisture content for infiltration and exfiltration scenarii respectively, with the two pressure differences.

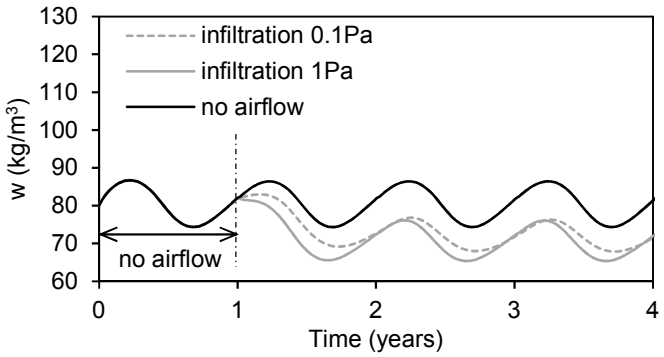

Figure 11: Averaged moisture content of wood bottom plate for infiltration

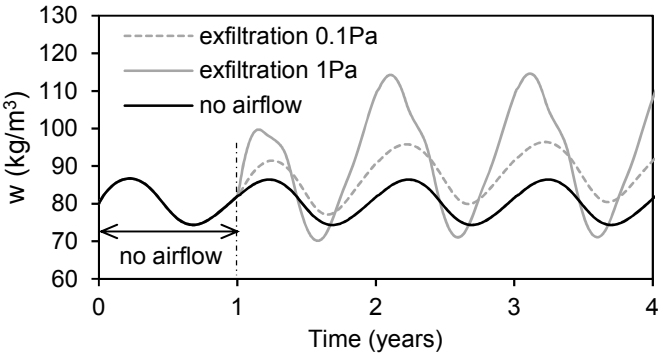

Figure 12: Averaged moisture content of wood bottom plate for exfiltration

The four-year hygrothermal simulation with no air flow shows that the assembly reaches periodic hygric equilibrium after one year. Moisture content is fluctuating with an amplitude of 5 kg/m^3 around its mean value is of 80 kg/m^3. Beginning at the end of the first year, the HAM simulation of the infiltration scenario shows drying of the wood bottom plate. In this case, two years are needed to reach hygric equilibrium at around 72 kg/m^3 for the flowrate corresponding to $P_{inside} - P_{outside} = -0.1$ Pa. For $P_{inside} - P_{outside} = -1$ Pa, the drying process is slightly more pronounced with an averaged moisture content of 70 kg/m^3. For both flow rates, moisture content amplitudes are very close to those observed without air flow.

The exfiltration scenario (fig. 12) shows opposite tendencies. The exfiltrated air flow causes a significant increase in moisture content in the wood bottom plate. For $P_{inside} - P_{outside} = 0.1$ Pa, the equilibrium moisture content increases by 20 kg/m^3 compared to the one without air flow. For $P_{inside} - P_{outside} = 1$ Pa, the predicted moisture content reaches 100 kg/m^3 as mean value, with an amplitude of nearly 50 kg/m^3. When interior moist air exfiltrates through the air channel, it comes into contact with increasingly cold building components, which increases its relative humidity until saturation. When the saturation point is attained, water vapour conatined in the air condensates and humidifies the materials in contact. In our case, this phenomena occurs here in the lower corner of the wood bottom plate

These opposite tendencies in infiltration and exfiltration are depicted by snapshots of the 2D relative humidity field at the beginning of the fourth year (fig. 13).

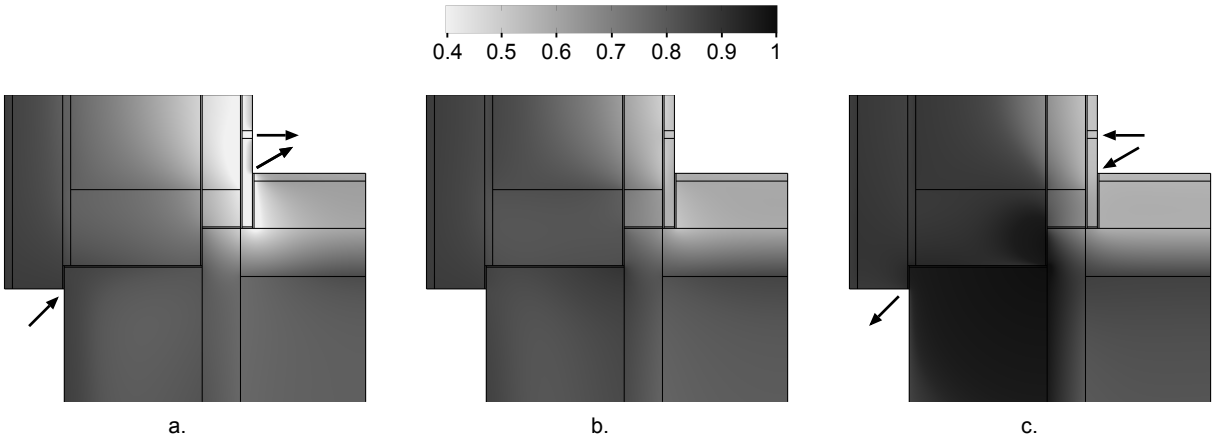

Figure 13: Relative humidity field in the beginning of the fourth year: in infiltration scenario (a.) or exfiltration scenario (c.) for $|P_{inside} - P_{outside}| = 1$ Pa, and without air flow (b.)

These results prove the strong coupling between velocity and hygrothermal fields, as well as marked tendancies depending on the flow direction. Infiltrating air flow dries the porous medium whereas exfiltrating air flow humidifies it. It appears that the moisturing process is much more significant than the drying one, even if the flowrates are similar. This can be explained considering two aspects:

- the non-linearity of the sorption curve: the more humid the material, the higher its hygric capacity.
- for high relative humidities, the liquid capillary flux becomes increasingly significant.

5. Conclusion

The current paper presents a numerical 2D model, HAM-Lea, for simulating heat air and moisture transfers through combined porous media and air channels. A one-domain approach is used: the same system of equations is used to describe HAM transfers in porous media and in air channels domains. Therefore, no boundary conditions between both domains are needed. This modelling strategy is thus particularly adapted for dealing with complex geometries. The model is successfully compared with one-dimensional numerical benchmark cases from literature. Finally, a complex 2D geometry combining porous media (air permeable or not) and thin air channels, is subjected to transient boundary conditions in relative humidity and temperature. Infiltration and exfiltration scenarii are tested on long time-periods. Results show a strong coupling between transfer processes, with a significant influence of the flow direction on the modification of the hygrothermal field. HAM-Lea can now be used within the field of building physics, to assess moisture safety of complex wall assemblies.

Acknowledgments

This work is financially supported by the French Environment and Energy Management Agency (ADEME), the Building Scientific and Technical Centre (CSTB), the French National Research Agency (ANR) through its Sustainable Cities and Buildings programme (MOB-AIR project n°ANR-12-VBDU-0009), and the Région Rhône-Alpes. The authors warmly thank Dr. Gilles Rusaouen from Université de Lyon for many fruitful discussions on CFD modelling.

Appendix: detailed description of the case study

Parameter	Material	Relative humidity φ [-]					
		0	**0.5**	**0.8**	**0.9**	**0.98**	**1**
water content $w(\varphi)$ [kg/m^3]	beton C12/15	0	35.0	53.0	73.8	149	175
	Fermacell	0	10.3	15.8	21.0	41.4	502
	wood fiberboard	0	8.10	19.0	23.4	36.7	980
	MDF board	0	50.0	70.0	85.0	145	667
	ext. finishing	0	1.58	6.20	13.5	57.7	220
	spruce	0	45.0	80.0	100	262	600
vapour resistance factor $\mu - factor$ [$-$]	beton C12/15	92					$+\infty$
	Fermacell	16					$+\infty$
	XPS	100					$+\infty$
	wood fiberboard	3					$+\infty$
	MDF board	12					$+\infty$
	ext. finishing	8.1					$+\infty$
	spruce	4.3					$+\infty$
moisture diffusivity $D_w(\varphi)$ [m^2/s] ($\times 10^{-12}$)	beton C12/15	20.0	200	217	237	14200	70000
	Fermacell	0	104	160	160	160	160
	XPS	0					
	wood fiberboard	0	85.3	200	290	565	20000
	MDF board	0	0.0532	0.0745	0.0904	44100	500000
	ext. finishing	0	0.0331	0.130	0.466	2.50	10
	spruce	0	23.3	53.3	70.5	209	500
thermal conductivity $\lambda_{mat}(\varphi)$ [W/(m.K)]	beton C12/15	1.60	1.80	1.91	2.03	2.47	2.62
	Fermacell	0.32					
	XPS	0.03					
	wood fiberboard	0.042	0.043	0.045	0.045	0.047	0.175
	MDF board	0.10	0.114	0.120	0.124	0.141	0.289
	ext. finishing	0.9	0.908	0.933	0.971	1.21	2.06
	spruce	0.23	0.26	0.28	0.30	0.40	0.62
dry thermal capacity c_{mat} [J/(kg.K)]	beton C12/15	850					
	Fermacell	1200					
	XPS	1500					
	wood fiberboard	2000					
	MDF board	2000					
	ext. finishing	850					
	spruce	1500					
dry density ρ_{mat} [kg/m^3]	beton C12/15	2200					
	Fermacell	1153					
	XPS	40					
	wood fiberboard	155					
	MDF board	528					
	ext. finishing	1360					
	spruce	455					

Figure 14: Material properties

Parameter	Value
μ_{air} [Pa.s]	1.8×10^{-5}
$c_{p_{air}}$ [J/(kg.K)]	1006
ρ_{air} [kg/m^3]	1.2
R [J/(mol.K)]	8.314
δ_0 [s]	1.96×10^{-10}
ρ_w [kg/m^3]	1000
c_w [J/(kg.K)]	4.18
L_v [J/kg]	2491×10^3
M_w [kg/mol]	0.018
λ_{air} [W/(m.K)]	0.026
$k_{fiberboard}$ [m^2]	2.8×10^{-10}

Figure 15: Additional simulation parameters

References

[1] H. Glaser. Temperatur und Dampfdruckverlauf in einer homogen Wand bei Feuchteausscheiding. *Kältetechnik*, pages 174–181, 1958. 1

[2] H.M. Künzel and Kurt Kiessl. Calculation of heat and moisture transfer in exposed building components. *International Journal of Heat and Mass Transfer*, 40(1):159 – 167, 1996. 1

[3] John Grunewald. *Diffusiver und konvektiver Stoff- und Energietransport in kapillarporösen Baustoffen*. Ph.D. Thesis, Technische Universität Dresden, 1997. 1

[4] Prabal Talukdar, Olalekan F. Osanyintola, Stephen O. Olutimayin, and Carey J. Simonson. An experimental data set for benchmarking 1-D, transient heat and moisture transfer models of hygroscopic building materials. Part II: Experimental, numerical and analytical data. *International Journal of Heat and Mass Transfer*, 50(25–26):4915 – 4926, 2007. 1

[5] Daniel Zirkelbach, H.M. Künzel, and Beate Schafaczek. Dampfkonvektion wird berechenbar – Instationäres Modell zur Berücksichtigung von konvektivem Feuchteeintrag bei der Simulation von Leicht- baukonstruktionen. In *4th international symposium on building and ductwork airtightness & 30th AIVC conference*, pages 1–8, Berlin, Germany, 2009. 1

[6] Guylaine Desmarais, Dominique Derome, and Paul Fazio. Mapping of Air Leakage in Exterior Wall Assemblies. *Journal of Thermal Envelope and Building Science*, 24(2):132–154, October 2000. 1

[7] M.O. Abadie, E.U. Finlayson, and A.J. Gadgil. Infiltration heat recovery in building walls: Computational fluid dynamics investigations results. Technical report, Lawrence Berkeley National Laboratory, 2002. 1, 5

[8] Catherine Langlais, Eric Arquis, and Dave J. McCaa. A theoretical and experimental study of convective effect in loose-fill thermal insulation. *Insulation Materials: testing and applications, ASTM STP 1030*, pages 290–318, 1990. 1, 5

[9] Anne Silberstein, Catherine Langlais, and Eric Arquis. Natural convection in light fibrous insulating materials with permeable interfaces: onset criteria and its effect on the thermal performances of the product. *Journal of Building Physics*, 14(1):22–42, 1990. 1

[10] Hamed Saber, Wahid Maref, Hakim Elmahdy, Michael Swinton, and Rock Glatzer. 3d heat and air transport model for predicting the thermal resistances of insulated wall assemblies. *Journal of Performance Simulation*, pages 75–91, 2012. 1

[11] Fitsum Tariku, Kumar Kumaran, and Paul Fazio. Transient model for coupled heat, air and moisture transfer through multilayered porous media. *International Journal of Heat and Mass Transfer*, 53(15–16):3035 – 3044, 2010. 1

[12] Qinru Li, Jiwu Rao, and Paul Fazio. Development of HAM tool for building envelope analysis. *Building and Environment*, 44(5):1065–1073, May 2009. 1, 9

[13] A.W.M. (Jos) van Schijndel. Integrated modeling of dynamic heat, air and moisture processes in buildings and systems using SimuLink and COMSOL. *Building Simulation*, 2(2):143–155, 2009. 2, 9

[14] Gerson Henrique dos Santos and Nathan Mendes. Heat, air and moisture transfer through hollow porous blocks. *International Journal of Heat and Mass Transfer*, 52(9-10):2390–2398, April 2009. 2

[15] Carlos G. Aguilar-Madera, Francisco J. Valdés-Parada, Benoît Goyeau, and J. Alberto Ochoa-Tapia. One-domain approach for heat transfer between a porous medium and a fluid. *International Journal of Heat and Mass Transfer*, 54(9-10):2089–2099, April 2011. 2

[16] Lorenzo Nespoli, M. Bianchi Janetti, and Fabian Ochs. Comparing Different Approaches for Moisture Transfer inside Constructions with Air Gaps. In *COMSOL Conference Rotterdam*, 2013. 2

[17] Michele Bianchi Janetti. Assessment of the moisture risk in constructions including convection inside air cavities. In *10th Nordic Symposium on Building Physics*, pages 1038–1044, Lund, Sweden, June 2014. 2

[18] H.M. Künzel. Modeling Air Leakage in Hygrothermal Envelope Simulation, 2012. 2

[19] Andrès Litvak. Campagne de mesure de l'étanchéité à l'air de 123 logements RT2000 - Rapport final. Technical report, CETE de Lyon, 2005. 2

[20] A. Janssens. *Reliable control of interstitial condensation in lightweight roof systems: calculation and assessement methods*. Ph.D. Thesis, Departement of Civil Engineering, KU Leuven, Belgium, 1998. 3

[21] Jelle Langmans, Andreas Nicolai, Ralf Klein, and Staf Roels. A quasi-steady state implementation of air convection in a transient heat and moisture building component model. *Building and Environment*, 58:208–218, December 2012. 3, 4, 9
[22] Donald A Nield and Adrian Bejan. *Convection in porous media*. Springer, New York, 2006. 4
[23] R. Byron Bird, Warren E. Stewart, and Edwin N. Lightfoot. *Transport Phenomena*. John Wiley & Sons Ltd, 2nd revised edition edition, March 2007. 4
[24] ASHRAE. Chapter 26 - Heat, air and moisture control in building assemblies - Material properties. In *ASHRAE Handbook of Fundamentals*. 2013. 5, 6
[25] Adrian Bejan. *Convection heat transfer*. Wiley, Hoboken, New Jersey, fourth edition edition, 2013. 5
[26] Wanyu R. Chan, Phillip N. Price, Michael D. Sohn, and Ashok J. Gadgil. Analysis of US residential air leakage database. *Lawrence Berkeley National Laboratory*, 2003. 6
[27] G.S. Beavers and D. D. Joseph. Boundary conditions at a natural permeable wall. *Journal of Fluid Mechanics*, 30:197–207, 1967. 6
[28] Clément Belleudy and Ahmad Kayello. A heat-airflow model for simulating the effects of air leakage on the temperature field in porous insulation. In *10th Nordic Symposium on Building Physics*, pages 79–86, Lund, Sweden, 2014. 6
[29] Carl-Eric Hagentoft, A. S. Kalagasidis, B. Adl-Zarrabi, S. Roels, J. Carmeliet, H. Hens, J. Grunewald, M. Funk, R. Becker, D. Shamir, O. Adan, H. Brocken, K. Kumaran, and R. Djebbar. Assessment Method of Numerical Prediction Models for Combined Heat, Air and Moisture Transfer in Building Components: Benchmarks for One-dimensional Cases. *Journal of Building Physics*, 27(4):327–352, April 2004. 7, 11
[30] Hugo Hens. *Building physics heat, air and moisture: fundamentals and engineering methods with examples and exercises*. Ernst & Sohn, Berlin, Germany, 2012. 7, 14
[31] Fujio Kuwahara, Mitsuhiro Shirota, and Akira Nakayama. A numerical study of interfacial convective heat transfer coefficient in two-energy equation model for convection in porous media. *International Journal of Heat and Mass Transfer*, 44(6):1153–1159, March 2001. 9
[32] C. R. Buchanan and M. H. Sherman. A mathematical model for infiltration heat recovery. Technical report, Lawrence Berkeley National Laboratory, May 2000. 9
[33] H.M. Künzel. *Simultaneous Heat and Moisture Transport in building Component*. Ph.D. Thesis, Fraunhofer IBP, 1995. 10, 13
[34] COMSOL Multiphysics User's Guide- version 5.0, October 2014. 11
[35] CETE de Lyon. Carnets Prebat Mininfil, Mémento étanchéité - Construction Ossature Bois - Isolation Thermique Intégrée. Technical report, November 2010. 13